Electronic Supplementary Information (ESI) for

Efficient Asymmetrical Silicon-Metal Dimer Electrocatalysts for Nitrogen Reduction Reaction

Chuangwei Liu,[1] Haoren Zheng,[1] Tianyi Wang,[1, 2] Xiaoli Zhang,[3] Zhongyuan Guo,[2,*] Hao Li [2,*]

[1] Key Lab for Anisotropy and Texture of Materials, School of Materials Science and Engineering, Northeastern University, Shenyang 110819, China.

[2] Advanced Institute for Materials Research (WPI-AIMR), Tohoku University, Sendai 980-8577, Japan.

[3] School of Material Science and Engineering, Zhengzhou University, Zhengzhou 450001, China.

Keywords: *g*-C_3N_4; Si-Metal dimer; ENRR; Electrocatalysis; DFT

[*]***Corresponding author:***

Dr. Zhongyuan Guo

Email: zhongyuanguo2022@163.com

Prof. Hao Li

Email: li.hao.b8@tohoku.ac.jp

1. Catalysts models

A 2D (2×2) supercell of *g*-C_3N_4 was built and then optimized to the stable strucutre (a = 14.36, b = 14.35, α = β = 90°, γ = 120°), including the lattice constant. Then, heteroatom (Si or Metal) was substituted into the N_{v1} site and the optimized catalysts models were denoted as Si@C_3N_4 (shown in Fig. 1a) and M@C_3N_4 (including Mo@C_3N_4 and Ru@C_3N_4 as shown in Fig. S8). Additionally, Si and Metal were both substituted into two N_{v1} sites to build asymmetrical dimer catalysts and the optimized catalyst models were denoted as SiM@C_3N_4. The vacuum thickness of catalyst models along the z direction is set to 20 Å to avoid false interactions between periodic structures during geometry optimizations.

2. Scheme of ENRR on Si@C_3N_4

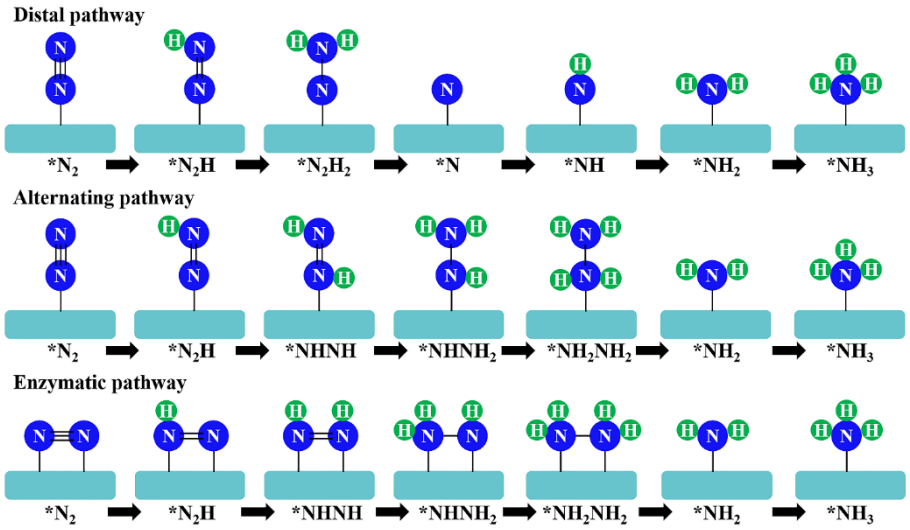

Fig. S1 The widely-proposed ENRR mechanisms, including distal, alternating and enzymatic ones.

3. Interstitial Si-doping into g-C_3N_4

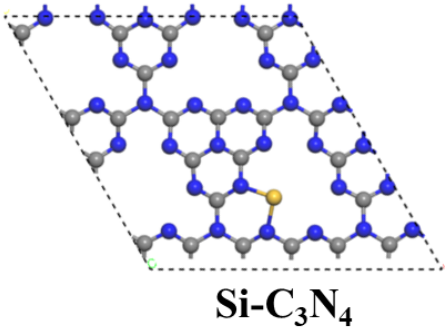

Fig. S2 The configuration of optimized Si-C_3N_4.

The formation energy of the configuration of Si-C_3N_4 is -0.02 eV, derived from the $E_f = E_{Si\text{-}C3N4} - \mu_{Si} - E_{g\text{-}C3N4}$, where $E_{Si\text{-}C3N4}$, and $E_{g\text{-}C3N4}$ represent the electronic energies of the catalyst and the pristine *g*-C_3N_4 substrate, and μ_{Si} refers to the chemical potential of Si, obtained by $1/n*E_{Si\text{-}cell}$. In comparison with the above configuration, the Si-doping into the Nv site (N_{v1}), named as Si@C_3N_4, is more energetically favorable.

4. SiM@C_3N_4 models

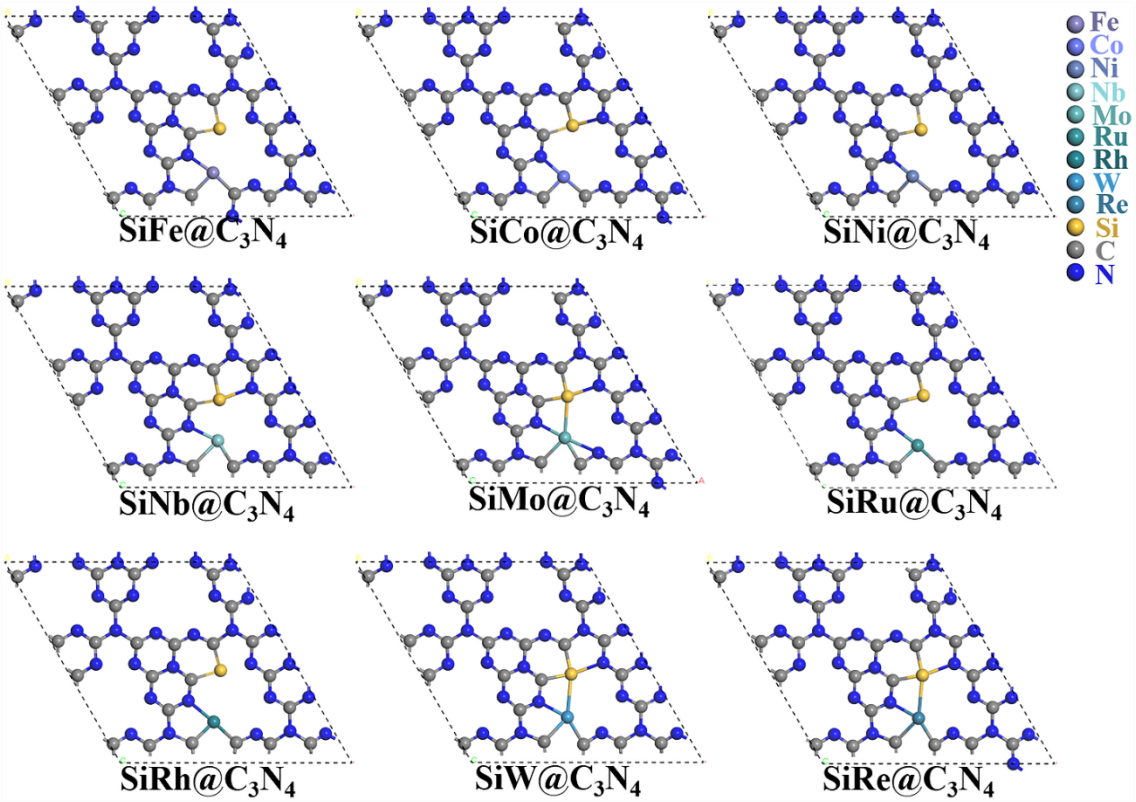

Fig. S3 The concept catalysts of SiM@C_3N_4.

5. Characteristics of $SiM@C_3N_4$

Table S1 Characteristics of $SiM@C_3N_4$.

Catalysts	Adsorption energy E_{ads}/eV		Binding energies of dopants, E_b/eV	Cohesive energies, $E_{co.}$/eV	Si-M bond length/Å
	end-on	side-on			
$Si@C_3N_4$	0.54	1.09	-6.51	-4.55 ($E_{co.Si}$)	—
$Mo@C_3N_4$	-0.77	0.01	-6.98	-5.86 ($E_{co.Mo}$)	—
$Ru@C_3N_4$	-0.24	—	-7.95	-6.77 ($E_{co.Ru}$)	—
$SiFe@C_3N_4$	—	0.16	-13.51	-5.14 ($E_{co.Fe}$)	2.82
$SiCo@C_3N_4$	—	-0.04	-13.91	-5.02 ($E_{co.Co}$)	3.23
$SiNi@C_3N_4$	—	0.43	-14.08	-4.70 ($E_{co.Ni}$)	2.99
$SiNb@C_3N_4$	—	0.12	-15.44	-6.78 ($E_{co.Nb}$)	2.86
$SiMo@C_3N_4$	—	-0.38	-14.18	-5.86 ($E_{co.Mo}$)	2.67
$SiRu@C_3N_4$	—	-0.29	-14.53	-6.77 ($E_{co.Ru}$)	3.11
$SiRh@C_3N_4$	—	0.34	-14.31	-5.66 ($E_{co.Rh}$)	3.24
$SiW@C_3N_4$	—	0.06	-15.58	-8.59 ($E_{co.W}$)	2.68
$SiRe@C_3N_4$	—	—	-15.09	-7.80 ($E_{co.Re}$)	2.67

6. N_2 adsorption on $SiRe@C_3N_4$ model

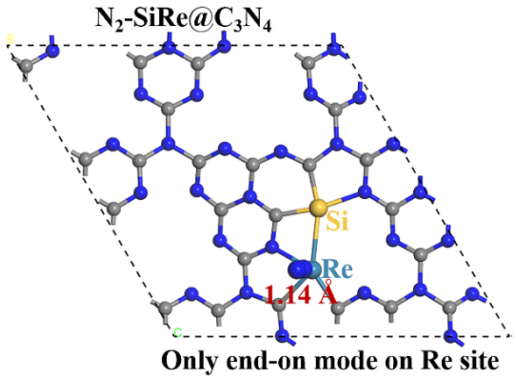

Fig. S4 N_2 adsorption on $SiRe@C_3N_4$.

7. Adsorption kinetics of N_2 on $SiM@C_3N_4$

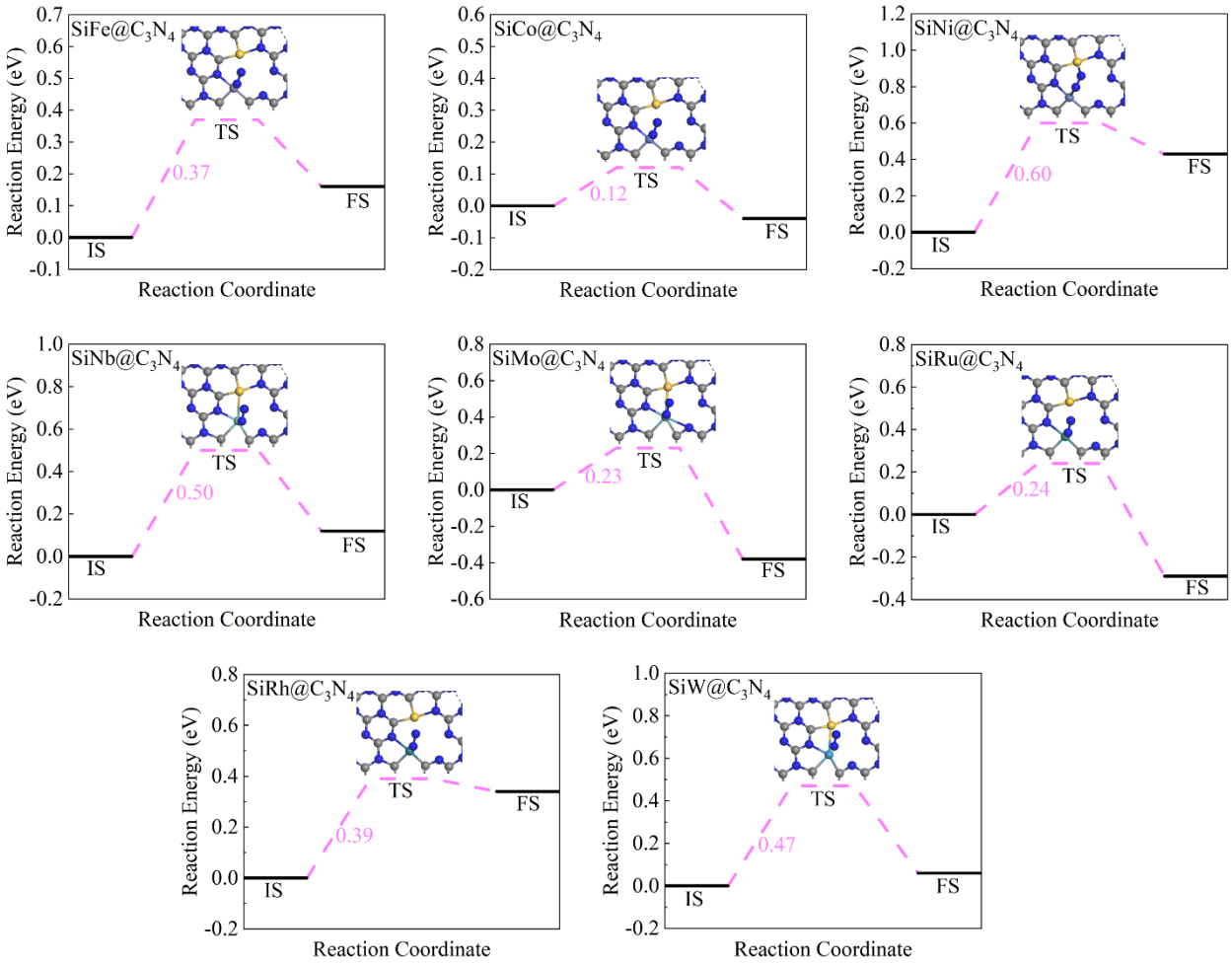

Fig. S5 The kinetics analysis of N_2 adsorption on $SiM@C_3N_4$ (inserts are the transition states). It is noticed that the TS was not analyzed for $SRe@C_3N_4$ because N_2 can merely be activated in the end-on configuration. The 'IS' and 'FS' terms refer to the initial and final states during the adsorption.

8. ENRR mechanisms on dimer catalysts

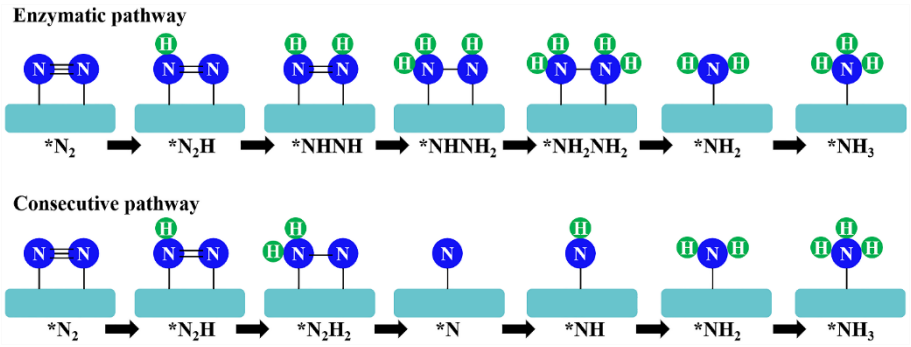

Fig. S6 The ENRR mechanisms on dimer catalysts.

9. ENRR pathways on SiRu@C_3N_4

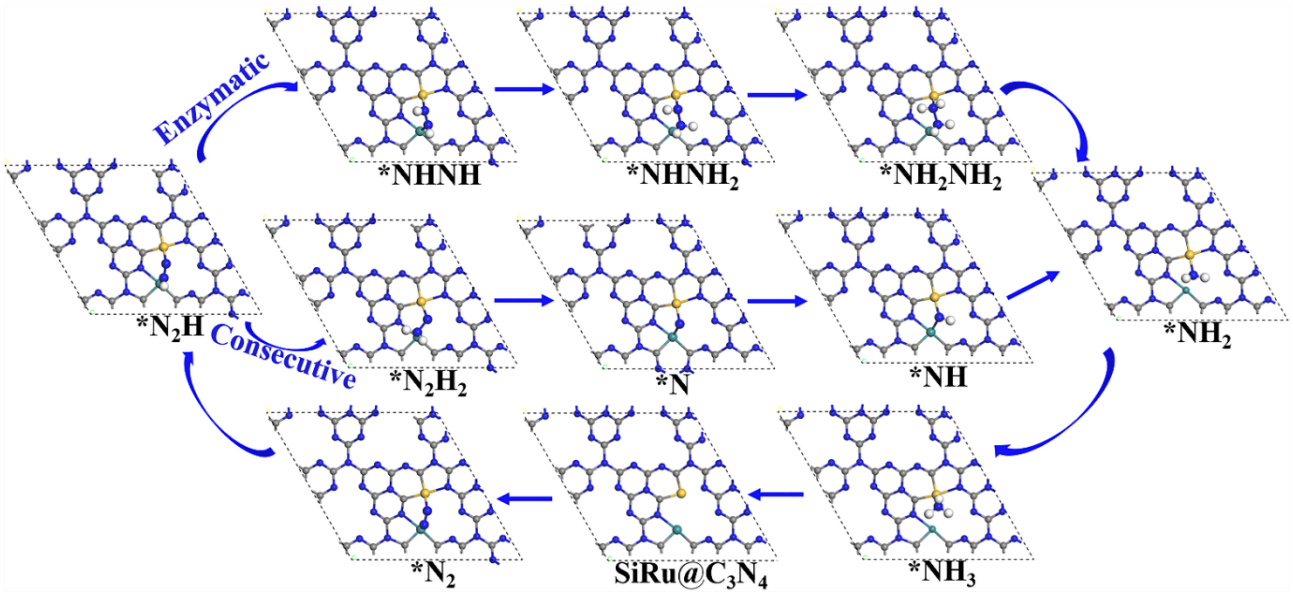

Fig. S7 ENRR enzymatic and consecutive pathways on SiRu@C_3N_4.

10. *N_2H on $SiMo@C_3N_4$ and $SiRu@C_3N_4$

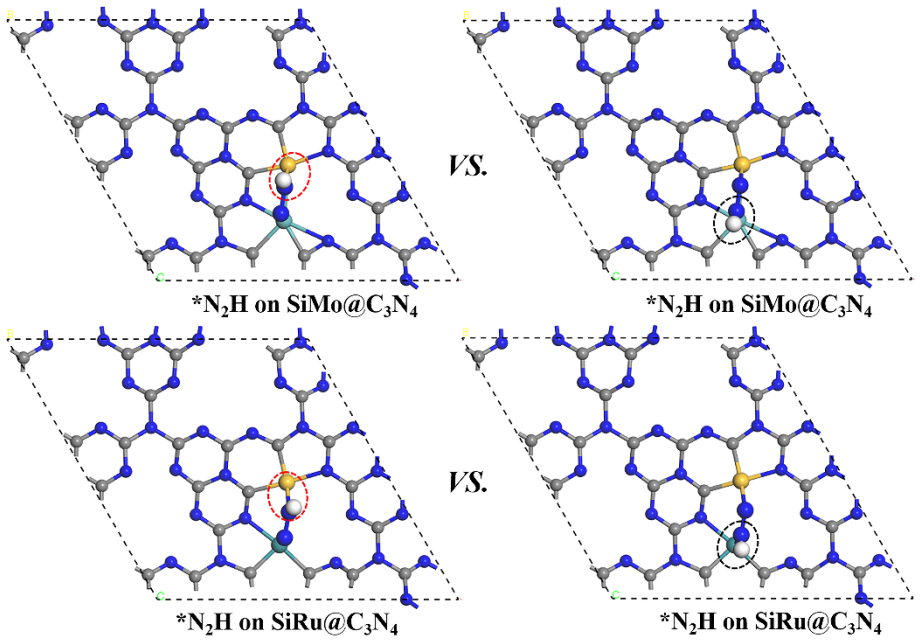

Fig. S8 The Si site *VS.* metal site (Mo/Ru) for the adsorption of *N_2H: the H^+/e^- pair tends to attack the N adatoms bound to the metal site energetically. The dash circles indicate different H adsorption sites on N adatom.

11. Mo@C_3N_4 and Ru@C_3N_4

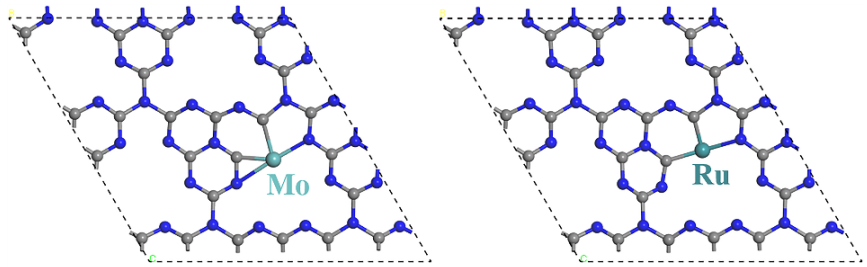

Mo@C_3N_4 **Ru@C_3N_4**

Fig. S9 The single-atom Mo/Ru catalysts supported on *g*-C_3N_4, named Mo@C_3N_4 and Ru@C_3N_4.

12. N_2 adsorption on $Mo@C_3N_4$ and $Ru@C_3N_4$

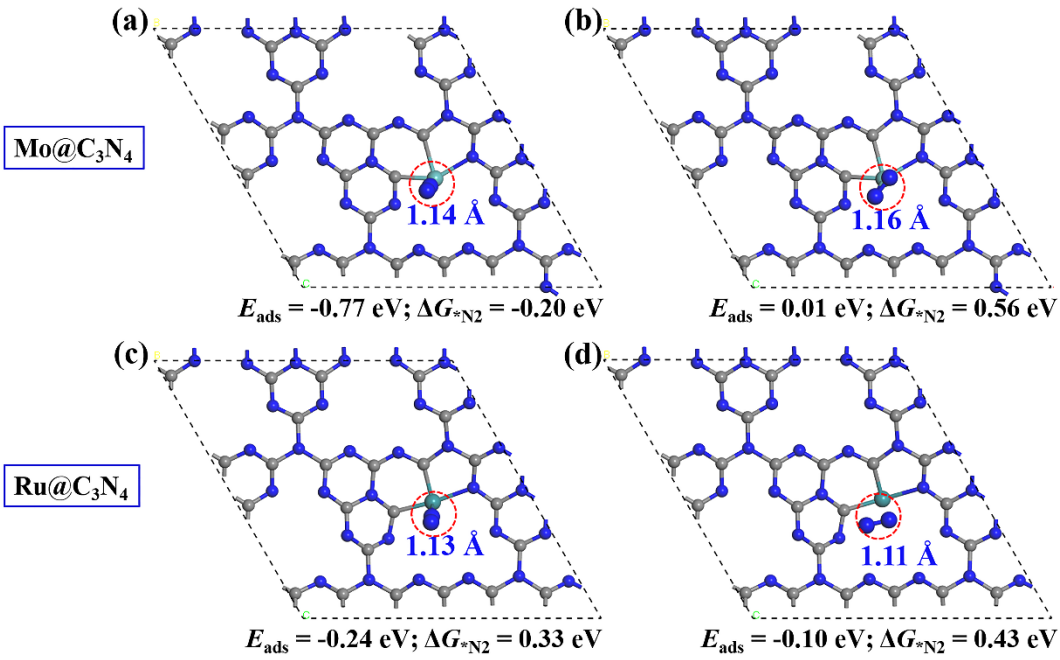

Fig. S10 The adsorption configurations of $*N_2$ on $Mo@C_3N_4$ and $Ru@C_3N_4$ with N-N bond lengths and energy changes.

13. ENRR on $Mo@C_3N_4$ and $Ru@C_3N_4$

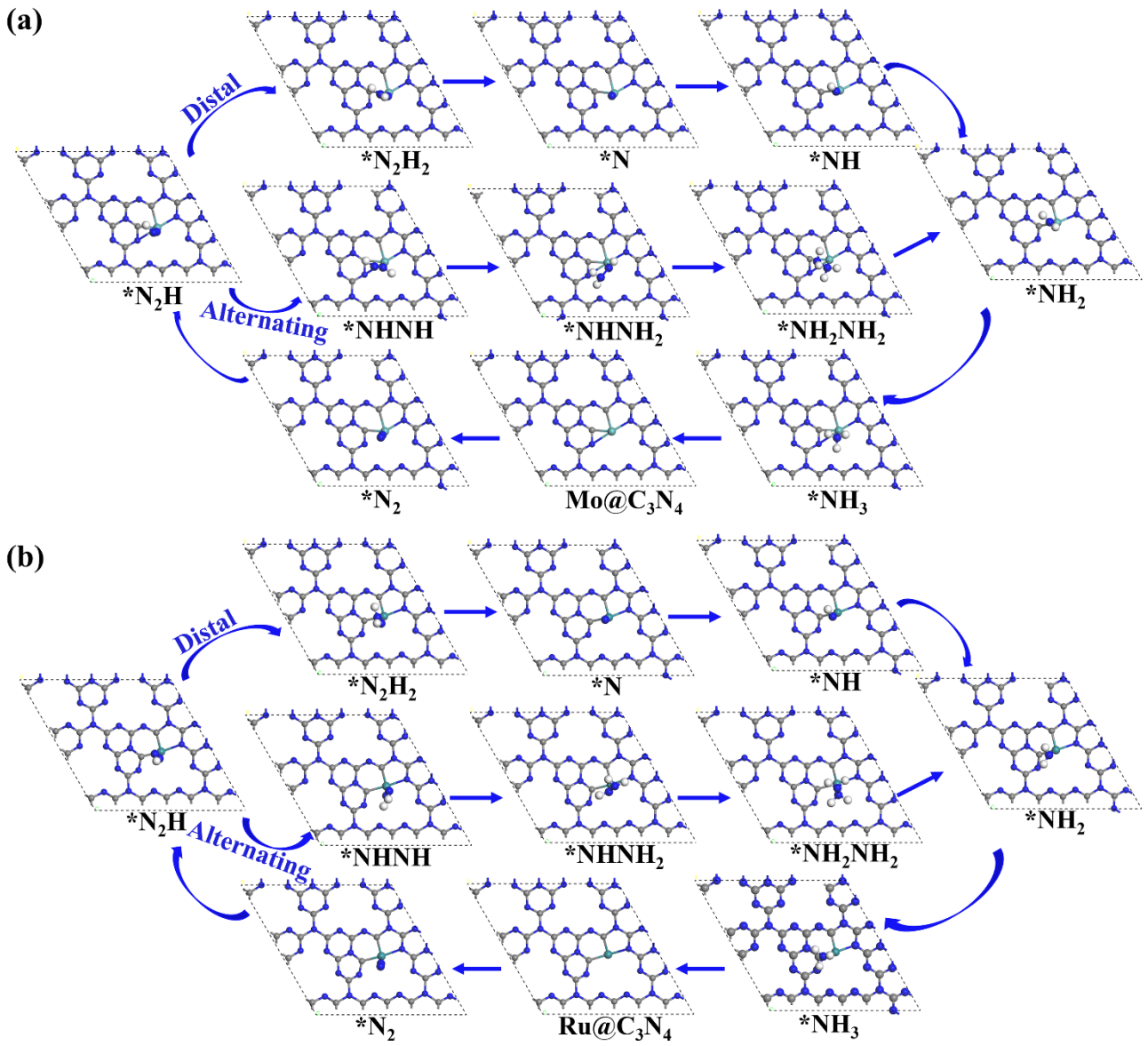

Fig. S11 ENRR intermediates along the distal and alternating pathways on (a) $Mo@C_3N_4$ and (b) $Ru@C_3N_4$.

14. Hirshfeld charge and N-N bond length analyses

Table S2 The Hirshfeld charge and N-N bond length analyses towards $*N_2$.

Catalysts	N-N bond/Å		Hirshfeld charges/e	
	End-on	Side-on	End-on	Side-on
$Si@C_3N_4$	1.13	1.21	0.06	-0.14
$Mo@C_3N_4$	1.14	1.16	-0.13	—
$Ru@C_3N_4$	1.13	—	-0.01	—
$SiMo@C_3N_4$	—	1.21	—	-0.20
$SiRu@C_3N_4$	—	1.20	—	-0.18

15. DOS and orbital analyses for N_2

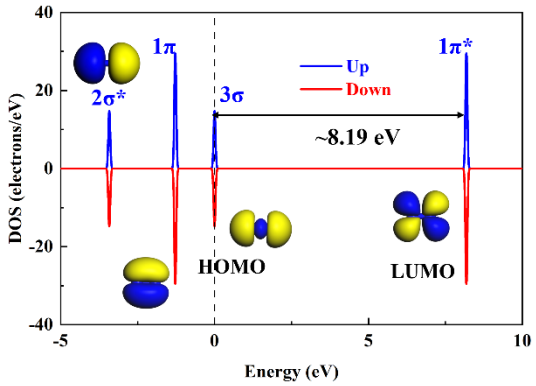

Fig. S12 DOS and orbital analyses for N_2.

From the above DOS image, it is noticed that the 3σ molecular orbital (MO) crosses the Fermi level. This image is produced by DMol^3 package, where the HOMO level is automatically corrected to the Fermi level. Therefore, it does not indicate that N_2 possesses metallic properties. Also, we did the orbital analysis shown in the above image, again evidencing the accuracy of DOS collected.

16. Evolution of Hirshfeld charges

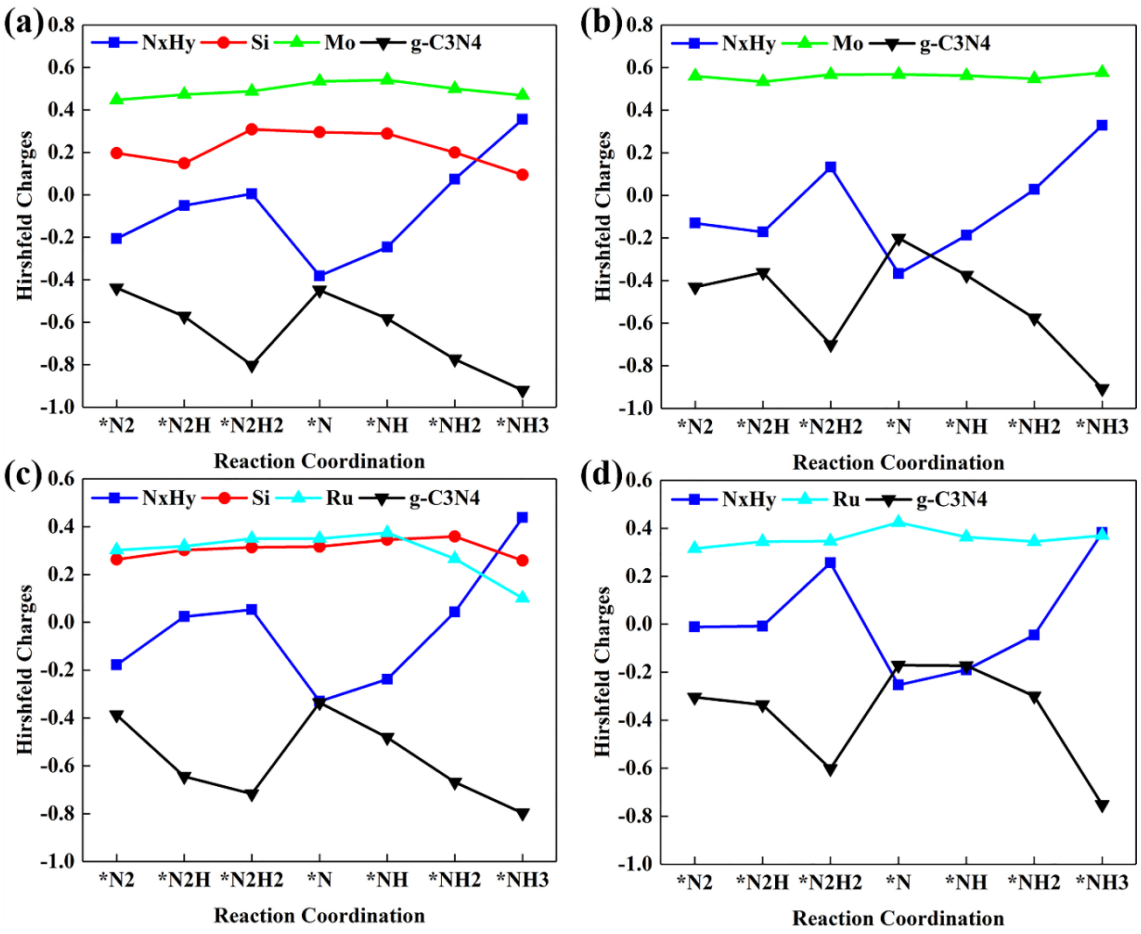

Fig. S13 (a, c) Evolution of Hirshfeld charges on SiMo@C_3N_4 and SiRu@C_3N_4 along the consecutive pathways; (b, d) Evolution of Hirshfeld charges on Mo@C_3N_4 and Ru@C_3N_4 along the distal pathway.

17. Energetically favorable configuration of dual Si-M dimer catalysts

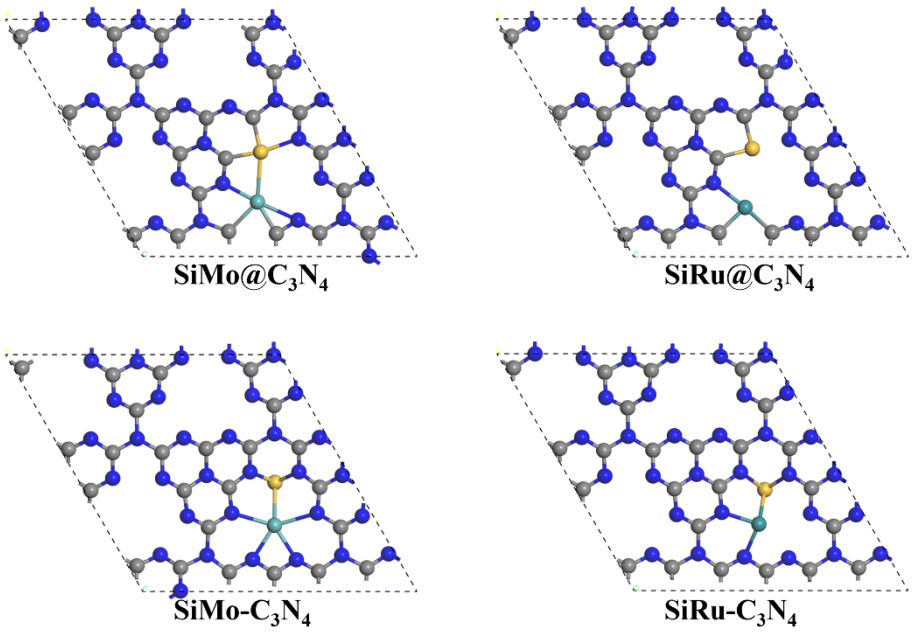

Fig. S14 Configurations of SiMo@C_3N_4 and SiRu@C_3N_4 vs. SiMo-C_3N_4 and SiRu-C_3N_4.

Here, we analyzed the formation energies of the above catalysts to evaluate the synthetic availability in labs. The dual-atom SiMo@C_3N_4 and SiRu@C_3N_4 catalysts designed by doping two dopant atoms into Nv1 vacancies are more energetically favorable than directly embedded into the hole of g-C_3N_4.

Table S3 Analyses of formation energies.

Concept-catalysts	$Si@C_3N_4$	$Si-C_3N_4$	$SiMo@C_3N_4$	$SiRu@C_3N_4$	$SiMo-C_3N_4$	$SiRu-C_3N_4$
Formation energy/eV	-0.08	-0.02	2.19	1.36	4.04	3.44

18. Thermodynamics calculated by DFT

Table S4 Thermodynamic quantities for H_2, N_2, and NH_3 gases at standard conditions ($N_2 + 3H_2 \rightarrow 2NH_3$).

Gases	E_{DFT}/eV	ZPE/eV	$\int C_P dT$	TS/eV	G/eV
H_2	-32.07	0.27	0.09	0.40	-32.11
N_2	-2981.80	0.15	0.09	0.59	-2982.15
NH_3	-1539.82	0.89	0.10	0.60	-1539.43

For the gas molecules, the Gibbs free energy calculation should be performed as follows:

$\mu = E_{DFT} + ZPE + \int C_P dT - TS$, where μ, E, and C_P denote the chemical potential, electronic energy, and heat capacity, respectively.

Table S5 Calculated data for ENRR.

Intermediates	Catalysts (SiMo@C_3N_4)		Catalysts (SiRu@C_3N_4)		Catalysts (Mo@C_3N_4)		Catalysts (Ru@C_3N_4)	
	E_{DFT}/eV	ZPE/eV	E_{DFT}/eV	ZPE/eV	E_{DFT}/eV	ZPE/eV	E_{DFT}/eV	ZPE/eV
*N_2	-83069.63	0.20	-83898.67	0.22	-76683.90	0.22	-77512.97	0.22
*N_2H	-83085.84	0.55	-83914.68	0.56	-76699.45	0.50	-77528.42	0.51
*N_2H_2	-83102.79	0.91	-83931.17	0.91	-76715.83	0.84	-77544.55	0.84
*N	-81579.12	0.11	-82407.32	0.095	-75192.60	0.10	-76020.32	0.09
*NH	-81595.77	0.40	-82425.16	0.43	-75209.12	0.37	-76037.32	0.36
*NH_2	-81612.72	0.53	-82442.03	0.75	-75225.72	0.68	-76054.91	0.70
*NH_3	-81629.54	1.08	-82457.92	0.90	-75242.59	1.06	-76071.55	1.08
*NHNH	-83102.39	0.86	-83931.14	0.86	-76715.42	0.86	-77544.53	0.66
*$NHNH_2$	-83118.94	1.22	-83947.86	1.24	-76732.20	0.99	-77561.17	1.18
*NH_2NH_2	-83135.28	1.37	-83963.92	1.38	-76748.51	1.54	-77577.83	1.34